Reprinted from *J. Mol. Biol.* (1976) **104**, 387–410

Assembly of the Head of Bacteriophage P22: X-ray Diffraction from Heads, Proheads and Related Structures

William Earnshaw, Sherwood Casjens and Stephen C. Harrison

J. Mol. Biol. (1976) **104**, 387–410

Assembly of the Head of Bacteriophage P22: X-ray Diffraction from Heads, Proheads and Related Structures

WILLIAM EARNSHAW, SHERWOOD CASJENS†

Department of Biology, Massachusetts Institute of Technology
Cambridge, Mass. 02139, U.S.A.

AND

STEPHEN C. HARRISON

Gibbs Laboratory, Harvard University
Cambridge, Mass. 02138, U.S.A.

(Received 20 August 1975)

We have used electron microscopy and small-angle X-ray diffraction to study the three principal structures found in the head assembly pathway of *Salmonella* phage P22. These structures are, in order of their appearance in the pathway: proheads, unstable filled heads (which lose their DNA and become empty heads upon isolation), and phage. In addition, we can convert proheads to an empty head-like form (the empty prohead) *in vitro* by treating them with 0·8% sodium dodecyl sulfate at room temperature.

We have shown that proheads are composed of a shell of coat protein with a radius of 256 Å, containing within it a thick shell or a solid ball (outer radius 215 Å) of a second protein, the scaffolding protein, which does not appear in phage. The three other structures studied are all about 10% larger than proheads, having outer shells with radii of about 285 Å. Empty heads and empty proheads appear identical by small-angle X-ray diffraction to a resolution of 25 Å, both being shells about 40 Å thick. Phage appear to be made up of a protein shell identical to that in empty heads and empty proheads, within which is packed the DNA.

Some details of the DNA packing are also revealed by the diffraction pattern of phage. The inter-helix distance is about 28 Å, and the hydration is about 1·5 g of water per g of DNA. Certain aspects of the pattern suggest that the DNA interacts in a specific manner with the coat protein subunits on the inside edge of the protein shell.

Thus, the prohead-to-head transformation involves, in addition to the loss of an internal scaffold and its replacement by DNA, a structural transition in the outer shell. Diffraction from features of the surface organization in these structures indicates that the clustering of the coat protein does not change radically during the expansion. The fact that the expansion occurs *in vitro* during the formation of empty proheads shows that it is due to the bonding properties of the coat protein alone, although it could be triggered *in vivo* by DNA–protein interactions. The significance of the structural transition is discussed in terms of its possible role in the control of head assembly and DNA packaging.

† Present address: Department of Microbiology, University of Utah Medical Center, Salt Lake City, Ut. 84112, U.S.A.

1. Introduction

P22, a bacteriophage of *Salmonella typhimurium*, originally of interest because of its capacity to carry out generalized transduction (Levine, 1972), has recently been shown to be a useful system for the study of head morphogenesis and DNA encapsulation (Botstein *et al.*, 1973; King *et al.*, 1973). For this purpose it offers several advantages over T4, where phage head assembly was first examined (reviewed by Casjens & King, 1975). First, the head assembly pathway is simpler than that of T4, involving only 11 genes. Second, major side pathways of assembly do not predominate when steps of the normal assembly pathway are blocked by mutation, making it easier to define the protein configurations relevant to assembly *in vivo*. Third, most of the structures are stable and easily isolated by gradient centrifugation. Fourth, the head and its assembly intermediates are isometric, facilitating detailed structural studies.

The pathway of P22 head assembly has been worked out in some detail by King *et al.* (1973). A simplified version of this pathway is shown in Figure 1. The earliest observed head-related structure is the prohead (Fig. 2(a)). Proheads accumulate in cells infected non-permissively with phage mutants in genes *1*, *2* and *3*. They contain the phage coat protein, gp5, and a scaffolding protein, gp8, which does not appear in mature phage (Botstein *et al.*, 1973). They also contain several minor proteins, which make a relatively small contribution to the total mass. Proheads interact with the concatomeric phage DNA to form structures partially or completely filled with DNA, as seen in ultra-thin sections of infected cells (Casjens & King, 1974; Lenk *et al.*, 1976). If these structures are not acted on by the products of genes *10* and *26*, the structure loses its DNA during isolation, and appears in electron micrographs to be an empty shell (Fig. 2(b)). During the transition from prohead to DNA-filled head, gp8 (uncleaved) leaves the structure and is reused to form more proheads in combination with newly synthesized gp5 (King & Casjens, 1974). As shown below, proheads may also be treated *in vitro* with dilute sodium dodecyl sulfate to give structures very similar to empty heads (Figs 1 and 2(d)). The product of the action of genes *10* and *26* is a filled head. This becomes a viable phage upon addition of a baseplate, the product of gene *9* (Figs 1 and 2(c)).

We report here on structural studies of the various intermediates in P22 head assembly, relying primarily on small-angle X-ray scattering to determine the radial distribution of protein and DNA. The purpose of these experiments was to obtain information that might shed light on the process of DNA encapsulation. Our results show that there are two types of structures: the phage-related structures (phage, empty heads and SDS†-treated empty proheads), which all appear to have similar shells of gp5; and proheads, which are significantly smaller. An expansion in the outer shell must therefore occur during the transition from proheads to phage-related structures. We have also obtained information about the local packing of DNA in the phage head. We discuss the implications of our structural observations for the regulation of P22 assembly.

2. Analysis of X-ray Scattering from Solutions of Regular Particles

The experiments described below depend on measuring and interpreting the scattering of X-rays from solutions of P22 phage and head precursors. Portions of

† Abbreviation used: SDS, sodium dodecyl sulfate.

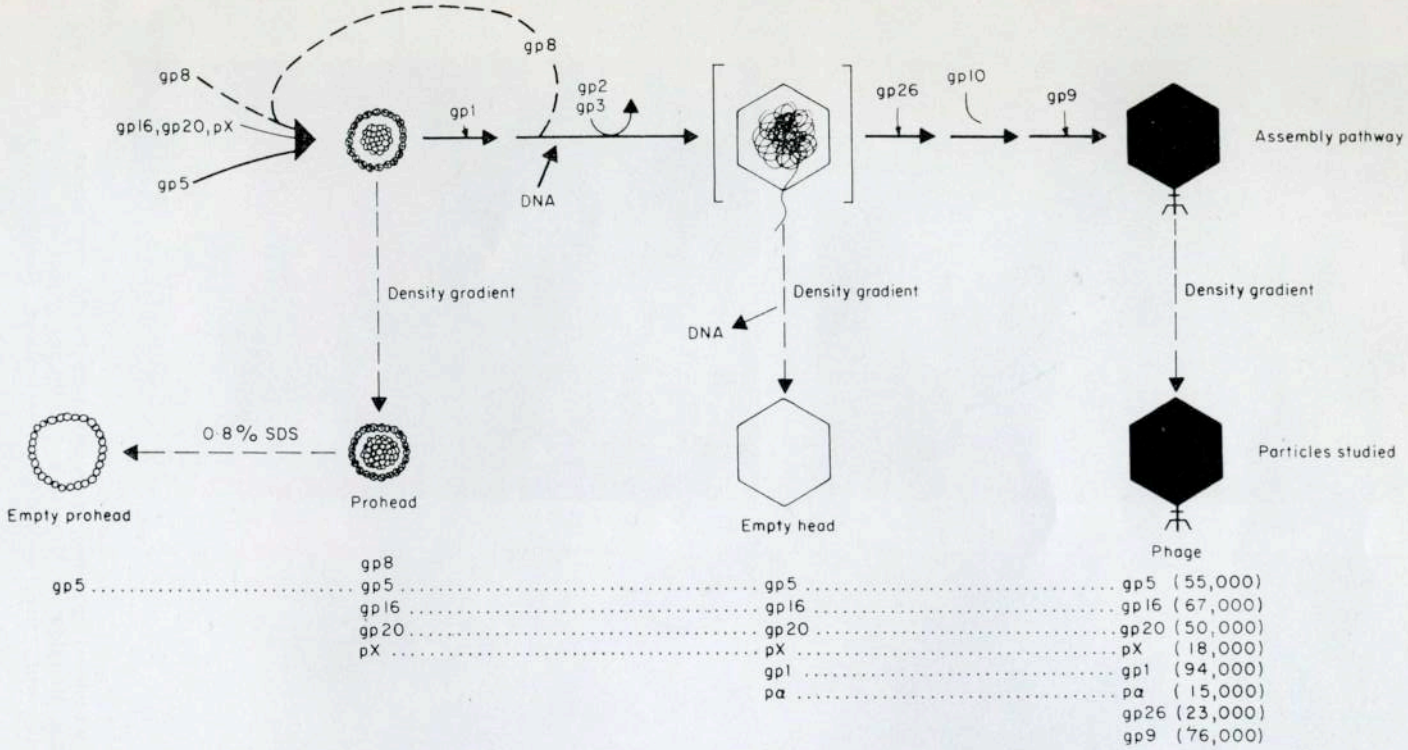

FIG. 1. P22 assembly pathway showing the relationships between the major observed structures.

This diagram summarizes the results in Botstein *et al.*, 1973; King *et al.*, 1973; King & Casjens, 1974; Casjens & King, 1974; and this paper. The particles labeled with names and whose protein compositions are shown are those studied in the present experiments. Empty heads and empty proheads are not actual precursors to phage, and this has been indicated by showing them below the assembly pathway. The size difference between proheads and the other structures has been exaggerated.

We have adopted the nomenclature of Casjens & King, 1975, for naming polypeptides. The letters gp denote a polypeptide identified both genetically and as a band in SDS/polyacrylamide gels. The letter p refers to a polypeptide which has been characterized only by the latter criterion. The protein composition of each particle studied is listed beneath it. The protein molecular weights are listed in the last column, except for gp8, which has a molecular weight of 42,000.

The biological events in P22 infection have been described by Botstein *et al.*, 1973; King *et al.*, 1973; King & Casjens, 1974; Botstein & Levine, 1968; and Tye *et al.*, 1974.

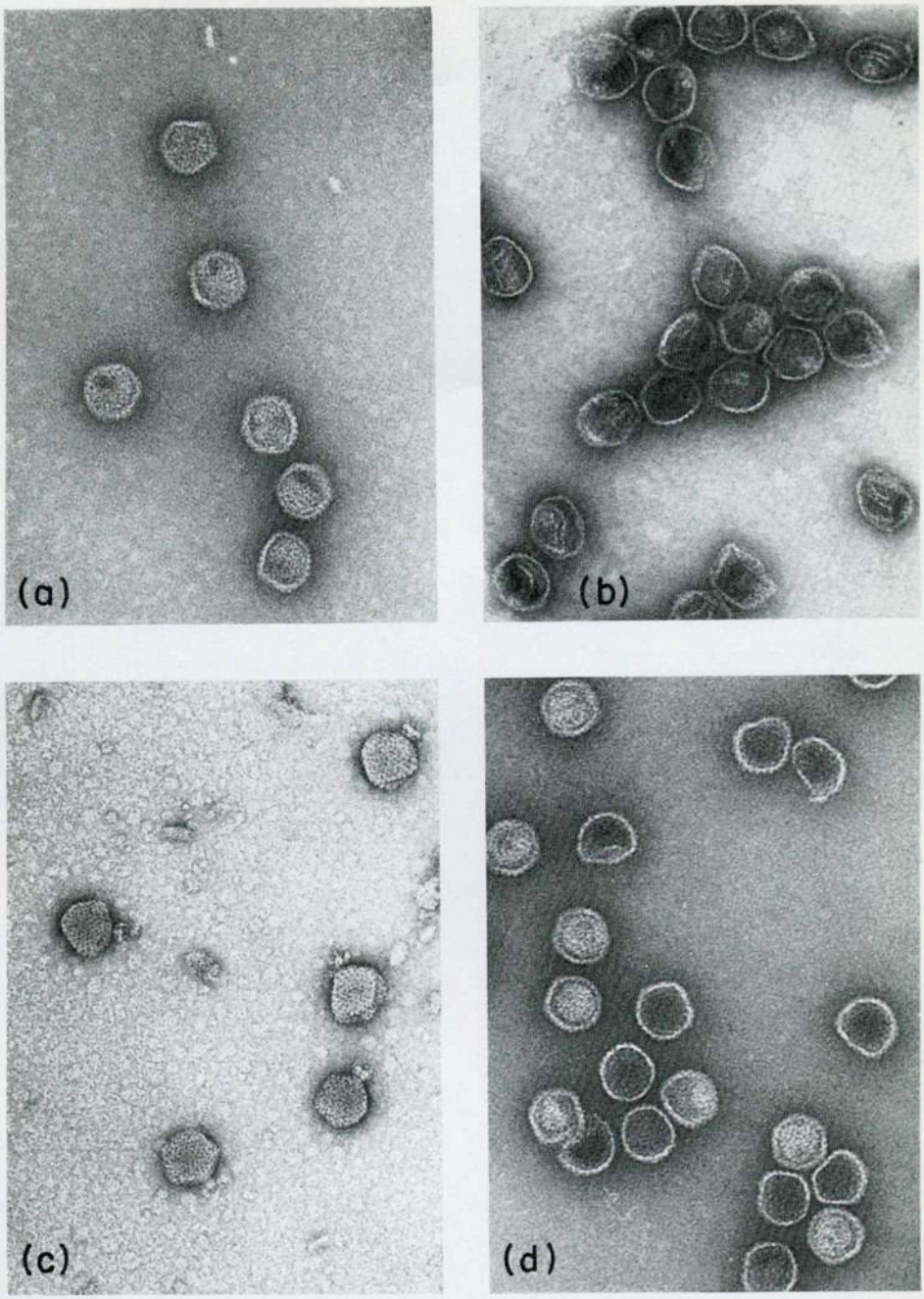

FIG. 2. The major P22 head-related structures, negatively stained with uranyl acetate. Particles were isolated as described in Materials and Methods section (b). (a) 3^- proheads; (b) 10^- empty heads; (c) P22 phage; (d) mixture of 2^- proheads and 2^- empty proheads. Magnification 126,000×.

the relevant theory have been presented by Finch & Holmes (1967), by Harrison (1969) and by Jack & Harrison (1975).

The intensity of radiation scattered from an unoriented specimen may be considered as the intensity scattered from a single particle, averaged over all angular orientations. For a particle in a given orientation, the amplitude and phase of the wave scattered in any direction may be determined by computing the Fourier transform of a function that describes the distribution of scattering density in the particle. The intensity of the scattered wave is then given by the square of the absolute value of this Fourier transform. For spherical structures like P22 heads, we represent the scattering density in spherical co-ordinates by $\rho(r, \theta, \phi)$. The function $\rho(r, \theta, \phi)$ may in general be considered as the sum of a spherically symmetric component $\rho_0(r)$, and a series of angularly dependent components, $\rho_n(r,\theta,\phi)$; $\rho_0(r)$ is just equal to the spherically averaged density, i.e. $\rho(r,\theta,\phi)$ averaged over all orientations.

The Fourier transform of $\rho(r,\theta,\phi)$ may likewise be considered as the sum of a spherically symmetric term, $G_0(R)$ which depends only on $\rho_0(r)$, and a series of higher-order terms which depend on the various $\rho_n(r,\theta,\phi)$ values. The variable, R, is a measure of the scattering angle: it is given by $R = 2\sin\theta/\lambda$, where θ is the half-angle of scattering and λ is the wavelength of the radiation. When the absolute value of the Fourier transform is squared and averaged over all possible orientations of the particle, in order to obtain the intensity scattered at any angle by an unoriented sample, a simple expression results:

$$I(R) = G_0(R)^2 + \sum_n G_n(R)^2, \tag{1}$$

where the $G_n(R)$ are terms that depend on the non-spherically symmetric components (ρ_n) of the particle density. Equation (1) thus states that *the scattered intensity may be considered as the sum of a series of independent terms, the first of which* (G_0) *depends only on the spherically averaged density in the particle* (ρ_0). Moreover, the terms that depend on non-spherically symmetric aspects of the structure, e.g. surface "bumps", "holes" between subunits, etc. can be shown to be zero for small values of R (for small scattering angles). If d is a characteristic distance between the bumps or holes in the structure, then $G_n(R) = 0$ ($n \neq 0$) for $R < 1/d$, and $G_0(R)$ is the sole contributing term.

The analysis proceeds in the following manner. The intensity of X-rays scattered from the sample is measured as a function of R. To a value of R roughly equal to the reciprocal of the distance between the largest bumps or holes in the structure, $I(R) = G_0(R)^2$, and the spherically averaged density in the particle ($\rho_0(r)$) may be computed directly from $G_0(R) = I(R)^{\frac{1}{2}}$. The form of $G_0(R)$ for these structures is like that of a cosine function with an amplitude that decreases with R. There is a maximum at $R = 0$ (the central maximum), then the function passes through a zero, a minimum, another zero, etc. When the function is squared, it gives a series of maxima (corresponding to both the maxima *and* the minima of G_0) and minima (corresponding to the zeros of G_0). These appear as concentric rings on the exposed X-ray film. There is an ambiguity in the sign of G_0 which can in favorable cases be resolved by reference to the principle of minimum wavelength (Bragg & Perutz, 1952). This principle states that the maxima of the transform of a bounded object succeed each other with a minimal distance of separation (minimum transform wavelength), determined by the overall dimensions of the object. We have been able to use this principle to resolve phase ambiguities in work reported here for the following reasons. From electron

micrographs of P22 and its intermediates, we can obtain an independent measure of the particle diameter. Moreover, the particles are sufficiently identical that the transform we observe has sharp and distinctly separated maxima and minima. In all cases, the separation of rings is such that were two successive rings to have the same sign, the distance between them (corresponding to a full transform wavelength) would require a particle diameter approximately twice as large as observed in the microscope (see Harrison *et al.*, 1971, for an example of a transform which could not be phased simply in the above manner). Having thus determined the relative signs in $G_0(R)$, and assuming the central maximum positive (since in all cases the mean density of the particles exceeds that of the solvent), we can calculate directly the spherically averaged electron density:

$$\rho_0(r) = 2\int_0^{R_0} G_0(R)\,[\sin(2\pi rR)/r]R\,dR, \tag{2}$$

where R_0 is the limiting resolution.

At large values of R (high resolution), the analysis becomes more complicated, since rings due to $G_n(R)$ are superimposed on the G_0 rings. When the $G_n(R)$ dominate, they limit the resolution to which $G_0(R)$ may be discerned and $\rho_0(r)$ computed. The question of distinguishing zero-order from higher-order terms is discussed by Harrison (1969) and by Jack & Harrison (1976). Where the G_n terms are weak, they appear as bumps in a monotonically decreasing intensity background. The higher-order terms contain interesting structural information, since they depend on the distribution of density as a function of θ and ϕ, i.e. on the distribution of surface features. It may seem paradoxical that the scattering from unoriented particles can yield information about non-spherically symmetric aspects of the structure: this results from the fact that the *intensity* (rather than the amplitude) is averaged in the scattering process.

Our present work relies largely on analysis of the spherically symmetric term, in order to compute the spherically averaged electron density in the P22 head-related structures. We have made only qualitative interpretations of the higher-order terms. Our structural interpretations are based largely on comparison of this spherically averaged density for P22 phage, proheads, empty heads and empty proheads (Fig. 1).

3. Materials and Methods

(a) *Bacterial and phage strains*

These were described previously by Botstein *et al.* (1973). The bacterial strains were DB74 (su^+) for preparing phage stocks, and DB21 (su^-) for preparation of the various mutant particles. The phage strains used are listed in Table 1.

(b) *Isolation of mutant particles*

The same basic protocol was followed in isolating all of the 4 types of particles studied. Bacteria (su^-) were infected with a multiplicity of 5 phage/cell. The infection was allowed to proceed for 2·5 h at 37°C, after which the cells were centrifuged, lysed with chloroform, and the solution cleared with pancreatic DNase. After low-speed centrifugation to remove debris, the resulting clear opalescent solution was concentrated by centrifugation through 15% sucrose (30% for phage) onto a CsCl shelf (density of 1·6 g/cm^3). Centrifugation (in an SW27.1 rotor with 18-ml buckets) was at 20,000 revs/min for 4 h for proheads, 25,000 revs/min for 2·5 h for phage and 25,000 revs/min for 5 h for empty heads. At the end of this step, phage, which had entered the CsCl as a tight band, were removed and

TABLE 1

Phage strains

Mutant particle produced	Genotype
Phage	P22 c_1^7 13$^-$*am* H101
Proheads	P22 c_1^7 3$^-$*am* N6 13$^-$*am* H101
	P22 c_1^7 2$^-$*am* H200 13$^-$*am* H101
	P22 c_1^7 1$^-$*am* N10 16$^-$*am* N121 20$^-$*am* N20 13$^-$*am* H101
Empty heads	P22 c_1^7 10$^-$*am* N107 13$^-$*am* H101

Genotypes and allele numbers of the phage strains used are listed above. The 13$^-$*am* allele prevents the phage from lysing the cell at the normal time. The c_1^7 allele is an absolute defective clear plaque mutant used to ensure that only lytic infections occur.

electron microscopic examination showed them to be virtually free of other particulate contaminants. Both proheads and empty heads were then layered (after dialysis) over a 15% to 30% sucrose gradient and centrifuged at 25,000 revs/min for 2·5 h (proheads) or 4 h (empty heads). When the bands were removed from this gradient, proheads were virtually pure (as seen in the electron microscope) and empty heads were contaminated 10 to 15% with proheads (a level of contamination too low to influence the X-ray results significantly). Empty proheads were isolated after treatment with SDS using a procedure identical to the second gradient for empty heads. The quality of all preparations was monitored by gel electrophoresis in the presence of SDS and electron microscopy. The buffer used for all samples was 0·01 M-Tris (pH 7·5), 0·005 M-$MgCl_2$.

(c) *Polyacrylamide gel electrophoresis*

Separation of the proteins of proheads and emptied proheads was achieved by polyacrylamide slab gel electrophoresis in the presence of SDS. The particles were disrupted and the proteins solubilized by boiling in 1% (w/v) SDS and 5% (v/v) 2-mercaptoethanol containing electrophoresis sample buffer (see O'Farrell *et al.*, 1973) for 1 min. Electrophoresis was carried out in slab gels as described by O'Farrell *et al.* (1973), and the proteins stained and gels scanned as described previously (Casjens & King, 1974).

(d) *Diffraction from intracellular phage*

S. typhimurium 7000 (*su*$^-$) cells were infected with a multiplicity of 10 phage (c_1^7 13$^-$ *am*) and the infection allowed to progress for 2 h at 37°C. In *su*$^-$ infection, this mutant forms phage particles but fails to cause cell lysis at the normal time. At 2 h (at which time there were 1500 viable phage/cell) the suspension was made 0·5% (w/v) in glutaraldehyde and placed on ice for 10 min, then incubated at room temperature for 20 min. At the end of the fixation step, the cells were pelleted and the pellet drawn into a quartz X-ray capillary. As a control, the procedure was also carried out with c_1^7 2$^-$ *am* 13$^-$ *am* phage-infected cells.

(e) *X-ray diffraction*

A concentrated solution of the particle in question was pelleted in an SW50.1 rotor (4·5-ml buckets) by spinning at 25,000 revs/min for 1·5 h or 17,000 revs/min for 4 h. (Identical results were obtained from pellets produced at different speeds.) The supernatant was removed as completely as possible, leaving behind a clear opalescent pellet. A portion of the pellet was drawn into a quartz capillary (outer diam. 0·7 mm, wall thickness 0·01 mm; Charles Supper Co., Natick, Mass.) and the capillary sealed with wax. X-ray photographs were taken with quartz-monochromatized CuKα radiation from an Elliott GX-6 rotating-anode microfocus X-ray tube. The mirror-monochromator camera (Huxley & Brown, 1967) had a specimen-to-film distance of approximately 12 cm. A

helium-filled tube was interposed between the sample and the film to reduce scatter and absorption.

Typical diffraction photographs are shown in Figs 4 and 5. The rings of scattered intensity correspond to successive maxima and minima in the transform of the spherically averaged electron density.

A number of specimens were checked by electron microscopy after X-ray exposure. No morphological changes were observed.

(f) *Intensity measurements*

Films were scanned on a 25 μm raster with a drum-type densitometer (Optronics International, Maynard, Mass.) which stored the optical densities on magnetic tape. The film intensity was integrated around concentric rings using a circular integration film-scan program (Harrison *et al.*, 1971). This program produces a plot of the scattered intensity (including background due to solvent and air scatter) as a function of radius in reciprocal space. The spacing of the intensity maxima was such that in all cases we could apply the principle of minimum wavelength (see above) and assume that the transform consisted of alternating positive and negative peaks. A baseline could therefore be drawn through the observed minima to correct for background, and transform amplitudes were obtained by taking the square root of the resultant corrected intensities.

The spherically averaged electron density profile was obtained by spherical Fourier inversion of these amplitudes.

Small errors in measured intensity, due to inexact scaling of successive films in a pack, incorrect baseline estimation, and other uncertainties, are amplified near the origin of the electron density profile by the spherical transformation. We do not attach any significance to the electron density profile at a radius less than the limit of resolution. The consequence of this for phage P22 (for example) is that we know nothing about the structure inside a radius of about 40 Å. Note that this volume is less than 0·4% of the total volume of the phage head.

Effects of interparticle interference were negligible except in the central maxima, which were in any case obtained by calculation (see below).

4. Results

(a) *Calculation of central and initial subsidiary maxima*

The spacing of the zeros in spherically averaged diffraction patterns varies inversely with particle radius. Our camera could resolve rings from particles as large as P22 intermediates, but the central maximum and often the first subsidiary maximum were obscured by the beam stop and not recorded. This information was supplied by the model-building approach used for tobacco mosaic virus by Franklin & Holmes (1958). The central maximum essentially provides a sloping baseline for the electron density profile. This is illustrated in Figure 3 where the effects of removing or doubling the central maximum are shown. Note that the removal of the central region is formally equivalent to doing dark-field microscopy: positions of detailed features are not altered, the only effect on the electron density profile being a lowering of the baseline towards the center. In order to determine the best estimate of the central maximum, we took (depending on the structure in question) the transform of either a solid ball or a spherical shell whose radius was calculated from the observed transform zeros (Guinier, 1963). Since our structures correspond fairly well to one or the other of these ideal types, the transform of the model and the observed transform were always fairly close, at least for the first few subsidiary maxima. The calculated transform was then scaled (i.e. the sloping baseline in Fig. 3 was raised or lowered) to give no negative electron density on the inside of the particle (since there are no

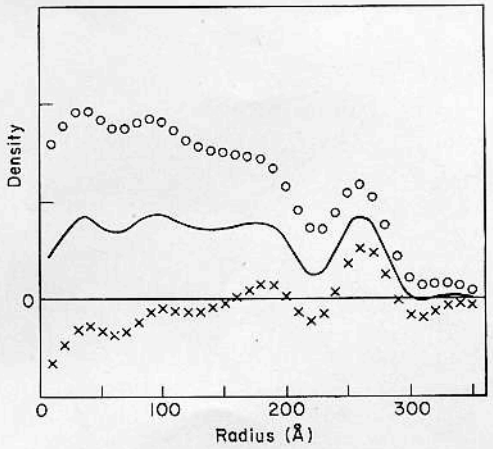

FIG. 3. Diagram showing the effects of changes in the central maximum of the diffraction pattern on the electron density profile.

The diffraction pattern of $1^{-}16^{-}20^{-}$ proheads was obtained as described in Materials and Methods section (e). It was phased as described in Analysis of X-ray Scattering from Solutions of Regular Particles and the central maximum and first two subsidiary maxima calculated as described in Results section (a). The solid line was obtained by spherical Fourier inversion (see Analysis of X-ray Scattering from Solutions of Regular Particles) of the phased transform, using the best approximation to the height of the central maximum obtained by calculation. The hollow circles indicate the result of doubling all the amplitude values of the central maximum prior to spherical Fourier inversion. The $\times$'s indicate the result of setting the entire central maximum equal to zero before inversion. It can be seen that the effect is roughly equivalent to adding a curved baseline to (or subtracting it from) the correct density profile.

known components of these particles less dense than water), while at the same time giving essentially zero density outside the particle (whose radius was estimated by electron microscopy). In the case of proheads, we used a more complex thick-shell model and refined by iterative trial and error until the above conditions were satisfied. This general procedure is justified because the criteria of non-negative density within the particle and zero density outside it are in practice strong enough to determine the scale of the central scatter.

It is important to note that in all cases the portion of the transform determined by calculation contributes only to very low resolution aspects of the density profile and does not influence fine detail.

(b) *X-ray diffraction from phage P22*

The small-angle X-ray diffraction pattern from phage P22 is shown in Figures 5(a) and 6(a). To a resolution of 64 Å, it is essentially identical to the pattern from a solid ball of uniform density and a radius of 307 Å. The rings in the central region correspond to successive maxima and minima in the solid-sphere transform. At a resolution of about 64 Å the rings become superimposed on a somewhat broader background ring. This represents scattering from non-spherically symmetric aspects of the structure. Beyond about 39 A, these components appear to predominate, limiting the resolution to which the spherically averaged electron density can be determined.

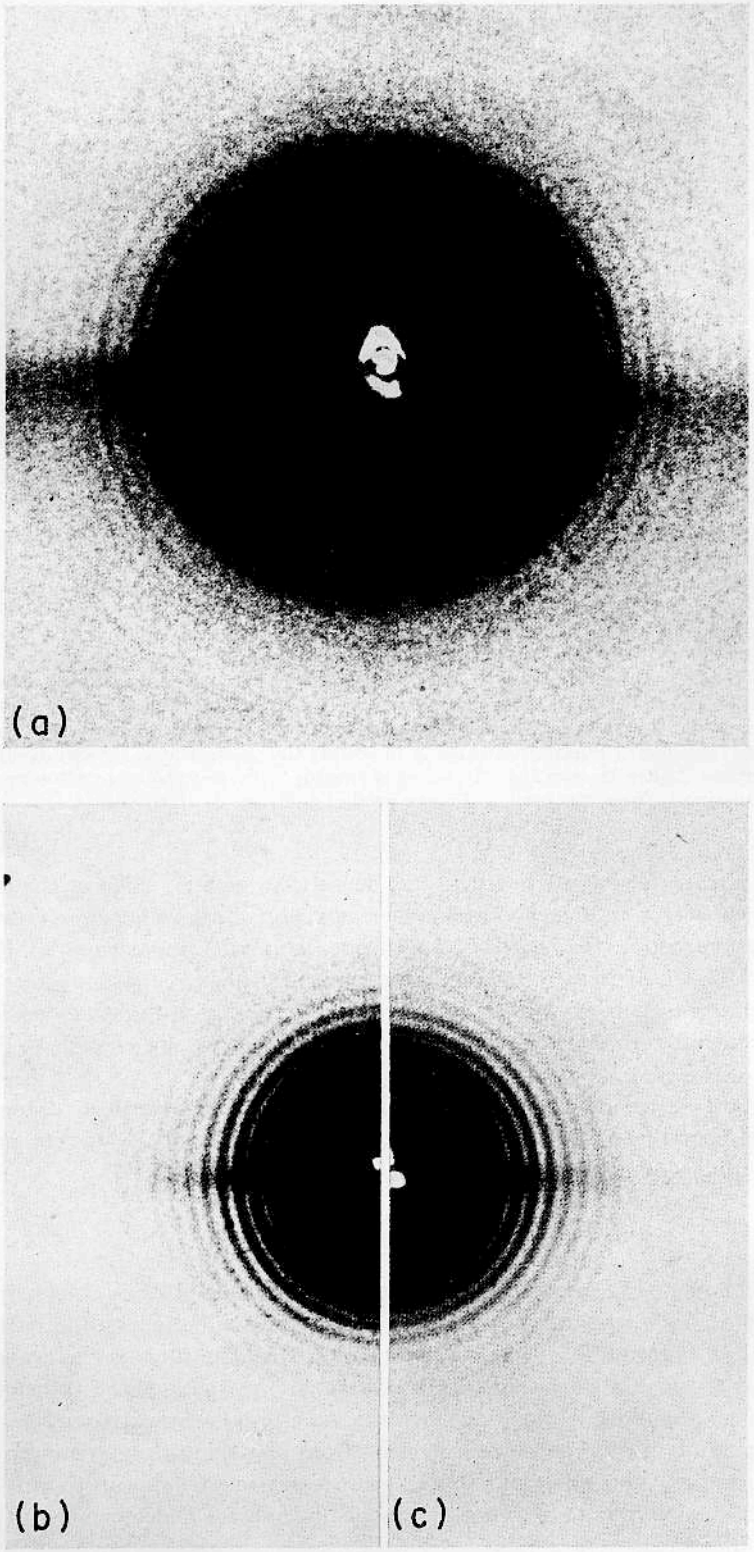

FIG. 4. Small-angle X-ray patterns from solutions of P22 head-related particles. The spherically averaged difffraction is observed as a series of rings. In both cases the central portion of the diffraction pattern is overexposed. (a) Empty heads, strong exposure; (b) empty heads, weaker exposure; (c) empty proheads. In all cases 1 cm = 0·004 $Å^{-1}$.

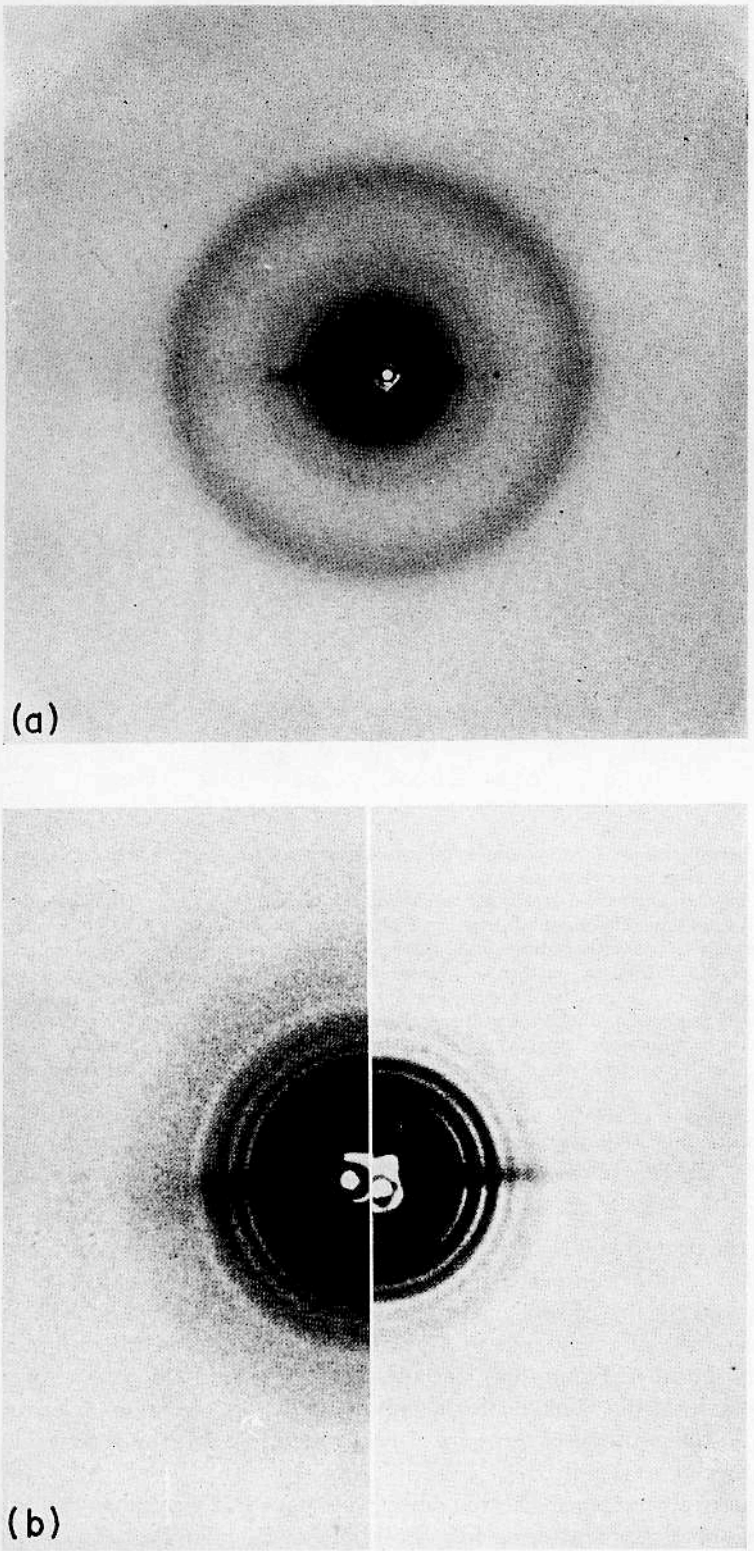

FIG. 5. As described in the legend to Figure 4. (a) Phage, 1 cm = 0·008 $Å^{-1}$; (b) 3⁻ proheads (strong and weaker exposure), 1 cm = 0·004 $Å^{-1}$.

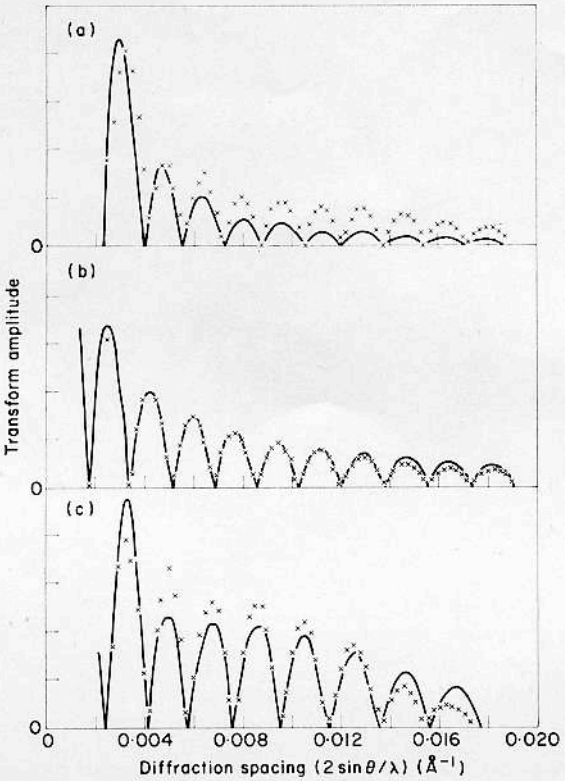

FIG. 6. Correspondence between observed transforms and the model transforms used to calculate the central and first subsidiary maxima.

In each case, the observed transform is shown as unconnected ×'s with the model diffraction plotted as a solid line. The model diffraction is shown as far in toward the origin as the scale of the ordinate (which is in arbitrary units) will allow. The abscissa represents the radial distance from the center of the diffraction pattern as measured on the film. The most important aspect of the agreement between observed and model transforms is the location of the zero points. This agreement is nearly perfect in all three instances.

The plots shown are as follows: (a) phage diffraction plotted with the diffraction from a sphere of radius 307 Å with a central hole of radius 35 Å; (b) 10^- empty head diffraction compared with that of a spherical shell of radius 289 Å; and (c) diffraction of 3^- proheads plotted with the diffraction from a solid sphere of relative density 0·75 and outer radius 200 Å centered within a shell of relative density 1·0 with inner radius 240 Å and outer radius 270 Å. (This latter model was arrived at empirically based on results from electron microscopy.)

Due to the problems (discussed in section (a)) encountered in measuring the central portion of the diffraction pattern, it was necessary to calculate values for the central maximum and the first subsidiary ring. The calculations were based on the expression for the transform of a solid sphere (Guinier, 1963), and scaled to the first observable ring. As is shown in Figure 6(a), the observed portion of the diffraction pattern is very similar to that calculated for a ball of radius 307 Å having a central hole of radius 35 Å: the positions of zeros are virtually identical, but the observed amplitudes fall off rather more rapidly.

The spherically averaged electron density in phage P22 was calculated as described in Analysis of X-ray Scattering from Solutions of Regular Particles, and the result

is shown in Figure 7(a). The profile is that of a shell of protein with a density maximum at 284 Å and an outermost radius of 314 Å containing a core of DNA with an apparent outer radius of 255 Å (see Table 3).

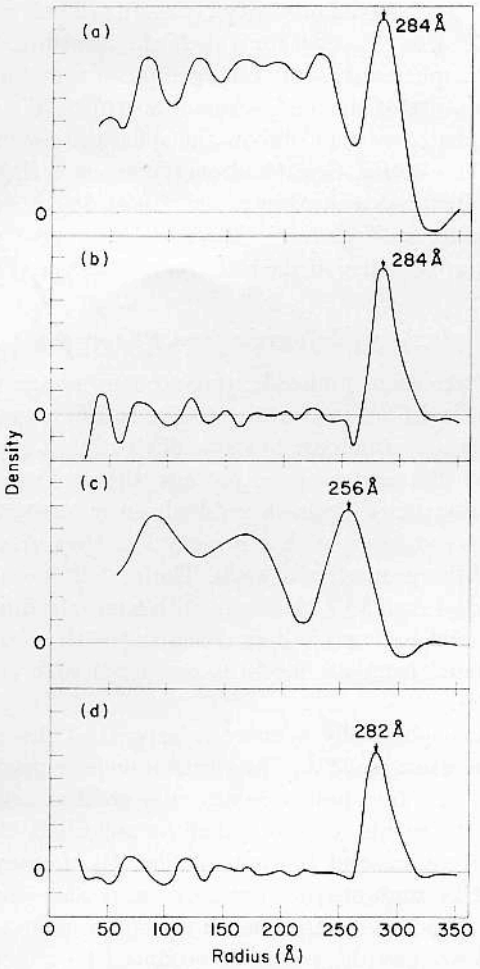

FIG. 7. Density profiles of P22 head-related structures.

The density profiles shown were obtained by spherical Fourier inversion of the phased diffraction amplitudes as described in Materials and Methods section (f) and Results section (a). The electron density is plotted in arbitrary units along the ordinate, and the radial distance from the particle center along the abscissa. The density was calculated at 10 Å intervals. Zero density on the ordinate corresponds to the density of buffer.

As was discussed in Materials and Methods section (f), the density profile is unreliable at spacings of less than the resolution to which it was calculated. Therefore the density profile is not drawn inside this radius. The resolution also tends to govern the apparent thickness of shells. (Note for proheads and phage that the shell thickness is the same as the resolution.) For this reason, these data cannot be taken as proof that proheads have a thicker outer shell than phage.

In all cases shown the central maximum was supplied by calculation; for phage, the first subsidiary maximum was also supplied.

The profiles shown are (a) phage to 39 Å resolution; (b) 10^- empty heads to 25 Å resolution; (c) 3^- proheads to 57 Å resolution; and (d) 2^- empty proheads to 25 Å resolution.

(c) *X-ray diffraction from P22 empty heads*

The diffraction from P22 empty heads, produced during non-permissive infection by phage mutated in gene *10*, is shown in Figures 4(a) and 6(b). It is very similar to the calculated diffraction from a thin spherical shell of radius 289 Å. It can be seen from Figure 6(b) that the observed intensity begins to fall below the calculated values beyond a spacing of 75 Å as expected for a shell of finite thickness.

Diffraction from non-spherically symmetric components first appears at a resolution of 64 Å. Due to the nature of the shell transform, which falls off much less rapidly than that of a solid sphere, we could follow the spherically symmetric term out to a resolution of 25 Å. The electron density of empty heads is shown in Figure 7(a), at 25 Å resolution. The shell has a maximum density at 284 Å and a profile that falls off somewhat less rapidly at large radii. The particles appear completely empty, in accordance with their appearance in the electron microscope (Fig. 2(b)).

(d) *X-ray diffraction from P22 proheads*

The diffraction pattern from proheads, produced by phage mutated in gene *3*, is shown in Figures 5(b) and 6(c). In contrast to the ball-like and shell-like transforms of phage and empty heads, which are systems of rings that get progressively lighter as one moves out from the center of the pattern, the prohead pattern is a series of almost equally dark rings that diminish suddenly in intensity at a spacing of 73 Å. This diffraction is not consistent with a density like that of a simple ball or shell; rather it has some of the properties of each. The best fit to model calculations was obtained with a spherical shell 30 Å thick and with a mean radius of 250 Å, containing centered within it a solid ball one-half as dense and with an outer radius of 200 Å. The transform calculated from the model is compared with that obtained from 3^- proheads in Figure 6(c).

Diffraction from non-spherically symmetric aspects of the structure appeared at 57 Å, limiting the resolution to 52 Å. The electron density profile is shown in Figure 7(c). The structure is best interpreted as an outer shell about 50 Å thick, of mean radius 256 Å, containing within it a thick shell (or solid ball, the two cannot readily be distinguished, cf. Materials and Methods section (f)) of outer radius 215 Å.

Proheads produced by mutants in other genes were also studied. Those produced by a mutant in gene *2* had an electron density profile similar to proheads from gene *3* mutants. The same was true for proheads produced by phage mutated in genes *1*, *16* and *20*. These particles lack three minor proteins (gp1, gp16 and gp20), while 2^- and 3^- proheads have the same protein composition as proheads isolated from wild-type infections (King *et al.*, 1973). Also identical was the structure of proheads prepared from cells lysed in a buffer of high ionic strength (0·3 M-NaCl). These results, together with those described above, are summarized in Table 3.

The above results show that there is an increase in radius that occurs during the transition from proheads to phage-related forms (phage, empty heads and empty proheads). Note that our measurement of this expansion is significant, even though it is somewhat smaller in magnitude than the limit of resolution to which the electron density profiles are known. This is because the uncertainty in *locating* an object is much less than the resolution limit. For example, the transform of a shell or a ball has an exact mathematical expression which is a function of the particle radius. (For a spherical shell the transform is given by the expression $\sin(2\pi aR)/2\pi aR$, where

a is the particle radius and R is the scattering angle, see Analysis of X-ray Scattering from Solutions of Regular Particles.) The position of zeros in the transform (minima in the intensity plot) thus gives a direct measure of the particle radius, independent of resolution.

(e) *Empty proheads*

Proheads contain two major proteins, gp5 and gp8, as well as much smaller amounts of the protein products of phage genes *1*, *16* and *20* (Botstein *et al.*, 1973; Casjens & King, 1974). They also contain one protein, pX, for which mutants have recently been obtained (Poteete, unpublished results). If these particles are placed in a solution of 0·8% SDS for 15 to 40 minutes at room temperature all of the proteins except gp5 are rendered soluble. Figure 8 shows SDS/polyacrylamide gel electrophoresis patterns of treated and untreated proheads, illustrating the essentially complete removal of the solubilized proteins.

If SDS-treated proheads (designated here empty proheads) are examined in the electron microscope with negative staining, they appear to be empty spherical shells (Fig. 2(d)) (Casjens & King, 1974). The diameter of the shells is similar to that of empty heads. The appearance of empty proheads in the electron microscope differs,

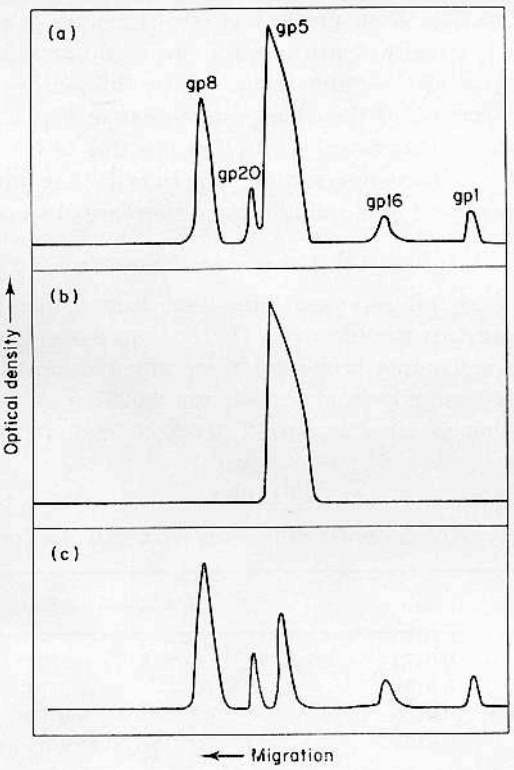

FIG. 8. SDS/polyacrylamide gel electrophoresis of 2⁻ proheads and empty proheads.

Proheads and empty proheads were prepared as described in Materials and Methods section (b) and Results section (d). Electrophoresis was as described in Materials and Methods section (c). After centrifugation, SDS-treated empty proheads were in the pellet, and SDS-released material in the supernatant. The tracings shown were smoothed by hand. (a) Untreated proheads; (b) SDS-treated empty proheads; (c) SDS-released material.

however, in two major respects from that of empty heads. First, they do not show visible vertices, seen in micrographs of empty heads. Second, they have the serrated outer edge characteristic of proheads; empty heads appear to have smoother edges (Fig. 2(b) and (d)). The reason for this difference is unclear, as X-ray data indicate that the surface clustering of coat protein subunits is the same in both types of particles (see Discussion).

SDS treatment of empty heads had no effect that could be detected by electron microscopy, SDS/polyacrylamide gel electrophoresis, or small-angle X-ray diffraction.

When empty proheads are examined in solution by small-angle X-ray diffraction, (Fig. 4(c)), they appear identical to empty heads. Figure 7(d) shows the electron density of 3^- empty proheads at 25 Å resolution. The electron density profile shows that empty proheads, like empty heads, are shells of radius 282 Å with virtually no internal electron density. This agrees with the observation by SDS/polyacrylamide gel electrophoresis, that mild treatment with SDS removes all gp8 protein from the particle.

(f) *Diffraction from intracellular phage*

On diffraction films from cells containing phage, there is a very strong region of diffuse scatter from the cells, obscuring much of the scattering from spherically symmetric aspects of phage structure. The two or three measurable maxima do correspond well to maxima from purified phage. Moreover, a strong ring at about 23 to 24 Å is observed virtually identical to the ring on diffraction patterns of purified phage particles. A scan of the outer region of the diffraction pattern is shown in Figure 9. The fine structure of this ring (not present in Fig. 9, since a coarse scan raster was used on the densitometer) shows that it is due to DNA packaged in intracellular phage heads (cf. Discussion section (c)). In cells that produce only proheads, phage DNA is not packaged, and no diffraction rings are observed.

(g) *Higher order diffraction*

On strong films from all samples, diffraction from non-spherically symmetric components of the structure was observed. On the films from phage-related structures (phage, empty heads and empty proheads), there were prominent rings at spacings of 0·0157, 0·018 (clearly seen only from phage), and 0·0237 $Å^{-1}$. Prohead films showed higher-order diffraction maxima at 0·0172, 0·020, 0·0267, 0·0322 and 0·0425 $Å^{-1}$.

TABLE 2

Location of peaks of higher-order diffraction from P22 head-related structures

Structure	Spacing (2 sin θ/λ)				
3^- Proheads	0·0172 ± 0·0005 $Å^{-1}$	0·0200	0·0267	0·0322	0·0425
10^- Empty heads	0·0159	—	0·0237		0·0386
2^- Empty proheads	0·0156	—	0·0239		0·0390
P22 phage	0·0157	0·0180	0·0235		0·0417

Positions of maxima were measured directly on films using either a microcomparator or a ruler. Certain higher order maxima occur at spacings linearly related to the particle radius. These values are listed in vertical columns. A dash means that the corresponding maximum could not be observed. The peak at 0·0417 $Å^{-1}$ from phage is due to the DNA. Superimposed on this broad peak is a series of narrow maxima located at spacings (in $Å^{-1}$) of 0·0311, 0·0329, 0·0346, 0·0366, 0·0384, 0·0403, 0·0420 and 0·0440.

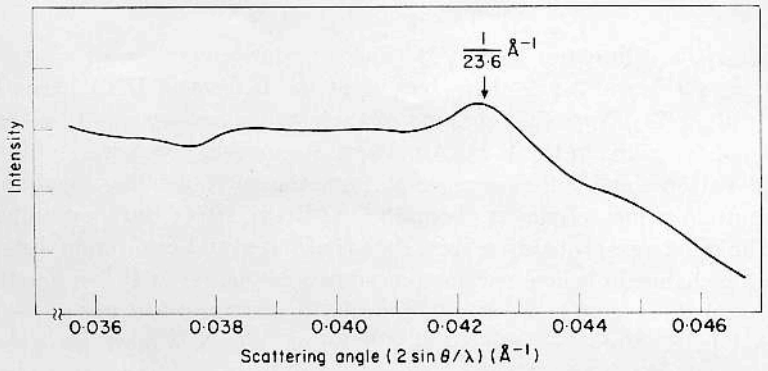

FIG. 9. Densitometer tracing of 24 Å ring seen in diffraction from a fixed pellet of cells containing approximately 1500 mature phage each. The scan raster used was 100 μm, which is too coarse to reproduce the fine structure of the peak. Ordinate: intensity (arbitrary units); abscissa: diffraction spacing ($Å^{-1}$). Note that the central portion of the pattern, which consisted of extremely strong diffuse scatter, is not shown.

The first three of these probably correspond to the three rings in the phage-related patterns, since they differ by just the proportional difference in size between phage and proheads (see Discussion, section (b)). The spacing of the first (1/58 $Å^{-1}$) agrees well with the distance between the serrated surface features seen in electron micrographs of proheads (Fig. 2(a)).

Phage diffraction patterns show a strong broad maximum near 0·042 $Å^{-1}$ (1/24 Å) with sharper maxima superimposed. Since this diffraction is not present in patterns from empty heads, it must be due to X-ray scattering by DNA. These data are summarized in Table 2.

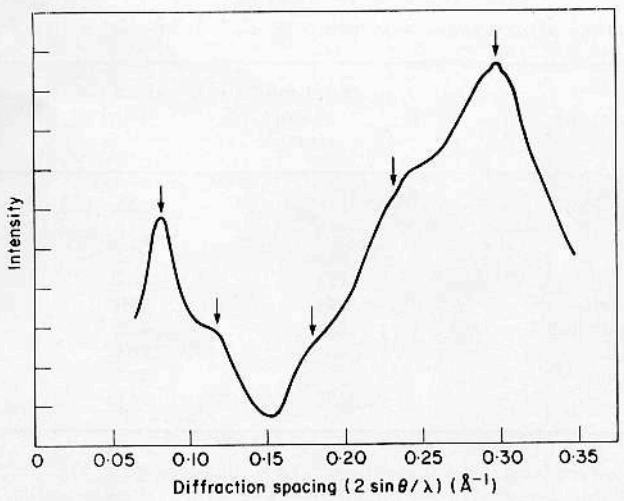

FIG. 10. Densitometer trace of wide-angle diffraction from P22 phage.

The specimen was made by inserting a pellet of phage directly into an X-ray capillary. Ordinate: intensity (arbitrary units); abscissa: diffraction spacing ($Å^{-1}$). Arrows indicate position of transform maxima, which are superimposed on a strong background due to solvent and to protein.

(h) *Wide-angle diffraction*

The wide-angle diffraction from P22 (Fig. 10) shows maxima at about 12·0 Å, 8·5 Å, 5·6 Å, 4·3 Å and 3·4 Å characteristic of the B form of DNA (Arnott, 1970; Maniatis *et al.*, 1974). Note that the first of these peaks corresponds to a maximum on the second layer-line in the B-DNA pattern: its spacing here agrees well with the classical B pattern, and differs somewhat from the corresponding maximum from DNA in solution (which occurs at about 13·5 Å; Bram, 1971; Harrison, unpublished results). The difference probably reflects details of water and counterion distribution, rather than a change in helical parameters, since a second-order Bessel function with a maximum in this region is sensitive primarily to structural features at the outside of the DNA helix. Moreover, the 3·4 Å diffraction, which is most sensitive to the stacking of nucleotide bases, is essentially identical in position and linewidth to the diffraction from DNA in solution as well as to the calculated B-DNA band. It differentiates most clearly from A or C-type structures.

5. Discussion

(a) *The spherically averaged structure of P22 head assembly intermediates*

The spherically averaged diffraction from phage P22 is essentially identical to the scattering from a solid ball of uniform density and of outer diameter about 307 Å. If we take the most likely model for the bacteriophage particle, a shell of protein enclosing a compact mass of DNA, our results suggest that this outer shell has a mean radius of 285 Å (determined from the outermost peak in the density profile and from a comparison with structures that have lost their DNA). The interior does not appear to have an electron density significantly higher than that of the protein,

TABLE 3

Summary of structural parameters of P22 head-related structures

Structure	Outer radius of inner structure	Mean radius of shell	Outer radius of shell
3⁻ Proheads	218±10 Å	256±5 Å	292±10 Å
	218	256	305
2⁻ Proheads	215	255	297
	214	257	294
1⁻16⁻20⁻ Proheads	224	260	302
1⁻16⁻20 Proheads in 0·3 M-NaCl	216	256	296
10⁻ Empty heads	—	284	316
2⁻ Empty proheads	—	282	314
P22 phage	255	284	314

These data are derived from density profiles similar to those shown in Fig. 7. The outer radius of the inner structure was measured at the minimum of the electron density profile. In proheads this inner structure is a core of gp8; while in phage it is the packaged DNA. There is no inner structure in empty heads and empty proheads. The mean radius of the shell is defined here as the radius of the maximum of the density profile. The outer radius of the shell is estimated from the base of the outer peak of the density profile. This is sensitive to the scaling of the central maximum, and as a result has somewhat greater scatter than the mean radius.

consistent with a composition of about 1·5 g of water per g of DNA (see Discussion of DNA structure below). The scaling of the central maximum (Results section (a) and Fig. 3) has some effect on the relative densities of inner and outer regions of the particle as seen in the electron density profile, but reasonable scale changes would not significantly alter the general shape of the profile.

Diffraction from empty heads shows that the structure is an empty shell, with a mean radius of 284 Å and a thickness of about 40 Å (Fig. 7(c)). Empty heads arise during the purification of unstable mutant heads (gene *10* mutants), which were partially or completely filled with DNA in the infected cell, but subsequently lost their DNA (Botstein *et al.*, 1973; Lenk *et al.*, 1976). We therefore expect the empty head to be similar in structure to the protein shell of phage.

Proheads are head precursors that accumulate when any of several assembly steps during DNA packaging are blocked by mutation (Botstein *et al.*, 1973). They are complex structures, composed of gp8 (the scaffolding protein, product of gene *8*), gp5 (the major coat protein, product of gene *5*), and several minor proteins. Protein gp8 is not found in mature phage: it serves as an assembly core, but unlike the case of phage T4 core protein, it is not cleaved during head formation. Rather, the gp8 molecules depart from the structure intact and are reused to form more proheads in combination with newly synthesized gp5 (King & Casjens, 1974). X-ray analysis indicates that proheads are composed of a shell of electron density with a mean radius of 256 Å, within which is a core with an outer radius of 215 Å.

It is clear from these results that purified phage and empty heads (which once contained DNA) have a mean radius for their protein shell about 30 Å larger than that of purified proheads. This expansion represents an increase in volume of about 30%. Our data indicate that the size difference holds for both intracellular and extracellular P22, since we observe identical diffraction from phage and infected cells in the 24 Å region. Were intracellular phage smaller but filled with the same complement of DNA, the interhelix distance and hence the spacing of this maximum would be correspondingly less (see section (c) below for a fuller interpretation of the 24 Å band). By contrast Dawson *et al.* (1975) reported that in thin sections of infected cells, petite λ and filled phage λ heads appeared to be the same size, while purified phage was larger. Note that if intracellular P22 were the size of proheads, the diffraction maxima would be at 19 Å and the interhelix spacing would be 22 to 23 Å, a distance characteristic only of rather dehydrated DNA fibers (Arnott, 1970).

Our measurements agree well with those of Lenk *et al.* (1975), who examined ultrathin sections of cells infected with various P22 mutants. They concluded that proheads had an outer shell with a radius of 275 Å and an inner shell with a radius of 190 Å. They also found that intracellular phage had a radius of 300 Å, about 10% larger than that of proheads, although they were not certain that the size difference was experimentally significant.

It is therefore likely that the prohead-to-phage transition (packaging and cutting of the phage chromosome) is accompanied by expansion of the protein coat as well as by loss of the internal scaffold (gp8). This increase in size during the transition from prohead precursor particles to DNA-filled particles may be a general phenomenon in phage assembly. The precursor particles of phage T4 (Simon, 1972), T7 (P. Serwer, personal communication) and lambda (Karamata *et al.*, 1962; Kaiser *et al.*, 1974; although Dawson *et al.*, 1975, suggest that the expansion may occur only after lysis) have all been found to be smaller than the completed phage particles. Our results

with SDS-treated proheads, which have lost the internal protein gp8, show that the increase in size is not due to the filling of the head with DNA, but is a property of the coat protein alone: it occurs spontaneously upon release of the scaffolding protein and the minor proteins. The internal protein thus appears to hold the coat protein in a more compact shell than it forms alone.

An analogous situation exists in the formation of the T4 phage tail, where sheath protein polymerizes in its uncontracted form only around an inner core (the tail core) (King, 1968). In both T4 tails and P22 proheads the outer layer has a second stable configuration (contracted sheath or expanded head), in which it can no longer interact with the core. The tail sheath contracts co-operatively when triggered by events at the baseplate (Moody, 1973). Similarly, expansion of the P22 head may proceed co-operatively when triggered by a perturbation of the prohead structure. In the *in vitro* experiment, SDS produces this perturbation; *in vivo*, it might be associated with initial interactions between the DNA and prohead. Since gp8 alone does not appear to form a stable assembly (King *et al.*, 1973; Casjens & King, 1974; Lenk *et al.*, 1975), expansion of the shell and release of gp5–gp8 contacts will cause the inner core to break apart into free gp8 subunits, which can then leave the particle. The existence of a second stable state for the outer shell therefore makes possible the recycling of gp8.

Comparison of the electron density profiles of proheads and empty proheads also shows directly that the internal material in proheads is gp8, since it is the only protein other than the coat protein present in amounts large enough to account for the observed electron density in the prohead interior. The alternative that proheads consist of an external shell of gp8 and an inner ball of gp5 that expands drastically after release of gp8, is unlikely on several grounds: (1) the relative amounts of gp5 and gp8 in proheads are known (Casjens & King, 1974) and are difficult to reconcile with the total relative volume in the inner core and outer shell of the prohead, respectively, but they are compatible with a model with internal gp8 and external gp5. (2) In the electron microscope (Fig. 2(d)) the outer shells of proheads and empty proheads show very similar serrated characteristics. (3) The relationship between the spacings of higher-order maxima from the two structures (which indicate features of the coat protein lattice, see discussion of surface organization, below) suggests a simple expansion with little alteration in surface-lattice packing.

If gp8 is in the prohead interior, an interesting problem in molecular geometry arises—how do approximately 250 molecules of the scaffolding protein ($M_r = 42{,}000$) leave the structure without disrupting it? Also, is this exit coupled either energetically or mechanically to DNA packaging?

(b) *Surface organization of P22 heads and head intermediates*

The organization of gp5 in P22 heads can probably be described by a $T = 7$ icosahedral surface lattice (Earnshaw & Casjens, unpublished results). Information about the surface organization is contained in higher-order diffracted maxima (see Analysis of X-ray Scattering from Solutions of Regular Particles). The various maxima ascribed to such features have been noted in Results section (h). In phage-related structures (phage, empty heads and empty proheads) the innermost observable higher-order ring occurs at a spacing of 0·0156 $Å^{-1}$ (i.e. 1/64 Å). In proheads this ring has a maximum at about 0·0172 $Å^{-1}$ (1/58 Å). The spacing in proheads is smaller than in phage-related structures by a ratio of 58/64 = 0·91, very similar to the ratio of the particle outer radii (295/314 = 0·94). We would expect such a proportionality

between the surface spacing and radius if the expansion from prohead to phage-related structures does not involve a major change in the surface clustering of subunits. That is, if the structure expands more or less uniformly, the distance between bumps on the surface will increase proportionally with the radius, and the higher order spacings will change correspondingly. Large changes in clustering will produce a new distribution of intercluster distances and a new set of diffraction maxima unrelated to the first. Some rearrangement must occur in the process in order to permit increased intercluster distances without loss of contact, but our results show that the changes involve relatively subtle reorientations rather than gross reorganization. Note that these arguments are independent of the particular triangulation number or mode of clustering present in P22.

(c) *DNA packing*

The wide-angle pattern from phage, dominated by DNA diffraction, shows that most or all of the DNA is in the B form. In the moderate angle region, there is a strong ring with a maximum at 1/24 Å. This ring is not present in diffraction from empty heads or empty proheads; it must therefore be due to DNA. It shows that the nucleic acid helices are packed in locally parallel arrays, and the width of the band indicates domains about 150 Å in lateral extent (Guinier, 1963). The 24 Å spacing corresponds to the largest Bragg spacing in this DNA lattice. It is slightly less than that observed in diffraction from so-called "ψ-DNA" precipitated by maximal concentrations of polyethylene oxide (25·3 Å; Maniatis *et al.*, 1974). If the DNA is locally hexagonally packed as in concentrated NaDNA gels (Luzzati & Nicolaieff, 1959), an inter-helix spacing of 28 Å would give rise to the observed 24 Å diffraction. As we would expect, this is greater than the mean interchain distance of 23 Å in crystalline fibers of B-form LiDNA at 66% relative humidity (Arnott, 1970). Diffraction at 24 Å has also been observed for T2, T7 and λ phage (North & Rich, 1961) and for purified T4 heads (Earnshaw, preliminary results).

As can be seen in Figure 7(a), the interior of the P22 phage particle has about the same electron density as the outer protein coat. From the average electron densities of DNA and water (0·59 and 0·33 e/Å^3, respectively), we calculate that a volume containing 1·5 g of water per g of nucleic acid will have a net density of 0·40 e/Å^3; this agrees well with the density of hydrated protein (Perutz, 1946; Harrison, 1969). We can also calculate the ratio of the weight of water to DNA from the local packing deduced above and the partial specific volume of DNA (Cohen & Eisenberg, 1968). The calculation is exactly analogous to the determination of the solvent volume fraction in protein crystals (Matthews, 1974). Assuming a local hexagonal unit cell for the packing of parallel DNA segments, with a lattice constant of 28 Å, we obtain a water content of 1·54 g per g of DNA, in excellent agreement with the estimate based on average density. Similar results would be obtained from any packing model (e.g. square or distorted hexagonal) consistent with the observed 24 Å intensity maximum.

Our measurement of the DNA packing distance also permits a rough calculation of the volume within the phage head occupied by DNA. The molecular weight of P22 DNA is 27×10^6 (Rhoades *et al.*, 1968), and the mass per unit length of B-DNA is approximately 190 daltons/Å. The total length of the P22 DNA molecule is therefore $1{\cdot}42 \times 10^5$ Å. Multiplying this by the area of the local unit cell deduced above, we obtain $9{\cdot}5 \times 10^7$ Å^3, equivalent to the volume of a sphere with radius 280 Å. Comparing

this with the density profiles of phage and empty heads (Fig. 7), we see that DNA fills the P22 head and that it is tightly packed throughout. Moreover, as discussed in section (a), this result implies that a full complement of DNA could probably not be accommodated in a smaller shell, e.g. the size of a prohead, since further "compression" of the DNA is unlikely at close to 100% relative humidity (cf. discussion of DNA hydration in Tunis & Hearst, 1968).

The short-wavelength "ripple" that modulates the 24 Å DNA ring has a periodicity characteristic of the internal diameter of the phage head. That is, the reciprocal spacing of the ripple maxima is 1/540 Å. Empty heads and empty proheads which are by other diffraction criteria isomorphous to the phage protein shell, do *not* give a similar set of maxima in the 24 Å region. Hence this diffraction cannot be ascribed simply to the superposition on the DNA band of diffraction ripples from some other part of the structure. It must be a consequence of packing DNA in the protein shell: either sampling of DNA diffraction or altered structural relationships in the protein. The strength of the individual ripples follows the profile of the 24 Å band, suggesting that the modulation represents a sampling of the DNA diffraction by a lattice-like function. The most straightforward interpretation is that X-rays scattered from DNA on opposite sides of the particle can interfere; that is, that segments of nucleic acid on opposite sides of the particle are in fixed positions with respect to each other and that this fixed relationship is the same in all particles. It seems to us implausible that the DNA, even if squeezed into a space just sufficient for packaging, has a long-range regularity like that in a single crystal without some interaction with the protein. A more plausible interpretation is that DNA interacts in a specific manner with subunits in the viral shell; this interaction, which need not be an extremely strong one, determines the position of those segments of packed DNA lying immediately against the protein. The fixed relationship of segments in opposite sides of the particle is then a consequence of the coherence and rigidity of the gp5 surface lattice.

6. Conclusion

Our major conclusions, discussed in the preceding section and incorporated in Figure 11, can be summarized as follows: (1) the prohead-to-head transformation in P22 involves, in addition to loss of a gp8 core, a structural transition in the outer gp5 shell. This transition involves an increase in radius but only small rearrangements in the particle surface. (2) Identical outer-shell structures are found *in vivo* after DNA incorporation and *in vitro* after mild treatment of proheads with SDS, indicating that the transition is a consequence of the bonding properties of gp5. (3) There is suggestive evidence for DNA–gp5 interactions in full heads.

Taken together, these conclusions suggest how interactions between the components of P22 might regulate its assembly. The gp8 core in proheads appears not only to nucleate formation of a gp5 shell, but also to hold the shell in a "tense" or metastable form that spontaneously rearranges when appropriately triggered. One reason for this rearrangement may be to allow for the exit of gp8. Likewise, in bacteriophage T4, cleavage and expansion of the coat protein, gp23, may be necessary to make core components susceptible to degradation (cf. Casjens & King, 1975). Moreover, if sites for P22 DNA–gp5 interactions are masked by gp8, then these sites will be unveiled co-operatively when the gp5 shell springs open. Interaction of DNA with sites thus exposed could be important in drawing it into the phage head. Indeed

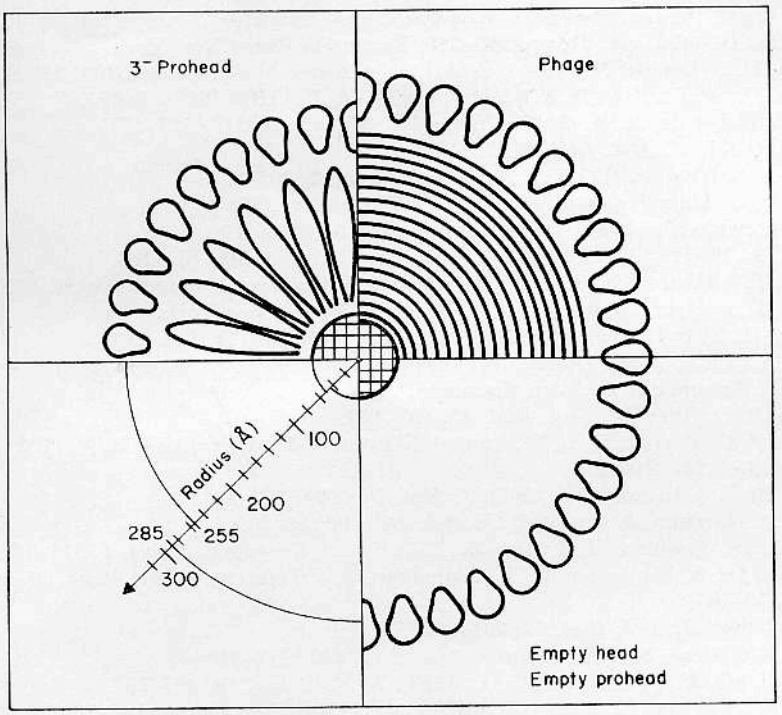

FIG. 11. Structures of P22 head-related particles.

The diagram shows a set of structures compatible with the density profiles in Fig. 7. The mean radii are indicated, and the subunit shape corresponds to a shell about 40 Å thick. We have no information about the innermost region shown crosshatched (cf. Materials and Methods section (f)). The shapes of subunits and the mode of DNA packing have been chosen arbitrarily.

the postulated masking of DNA binding sites by an internal structure can be generalized to other phage assembly pathways, where structural evidence for such interactions is presently lacking. Whatever the validity of these speculations, it is clear that a complex set of specific macromolecular interactions has evolved to regulate P22 assembly, and that further structural and biochemical studies are needed to describe them.

We are especially indebted to Jonathan King for impetus, interest, and support given to this work. We thank Elaine Lenk for able electron microscopy and photographic assistance, D. L. D. Caspar for the use of an Optronics film scanner, and Ruth Griffin Shea for the gift of a $c_1 13^- 1^- 16^- 20^-$ mutant. This work was supported by National Institutes of Health grants GM-17980 (to J. K.) and CA-13202 (to S. C. H.). Computations were supported by a grant from the Massachusetts Institute of Technology Health Sciences Fund (to J. K.). The authors were the recipients of a National Science Foundation predoctoral fellowship (to W. E.), a Helen Hay Whitney postdoctoral fellowship (to S. C.) and a National Institutes of Health Research Career Development award CA-70169 (to S. C. H.).

REFERENCES

Arnott, S. (1970). In *Progress in Biophysics and Molecular Biology* (Butler, J. A. V. & Noble, D., eds), vol. 21, pp. 265–319, Pergamon Press, New York.

Botstein, D. & Levine, M. (1968). *Cold Spring Harbor Symp. Quant. Biol.* **33**, 659–667.

Botstein, D., Waddell, C. H. & King, J. (1973). *J. Mol. Biol.* **80**, 669–695.

Bragg, L. & Perutz, M. F. (1952). *Proc. Roy. Soc. ser. A*, **213**, 425–435.

Bram, S. (1971). *J. Mol. Biol.* **58**, 277–288.

Casjens, S. & King, J. (1974). *J. Supramol. Struct.* **2**, 202–224.

Casjens, S. & King, J. (1975). *Annu. Rev. Biochem.* **44**, 555–611.

Cohen, G. & Eisenberg, H. (1968). *Biopolymers*, **6**, 1077–1100.

Dawson, P., Skalka, A. & Simon, L. (1975). *J. Mol. Biol.* **93**, 167–180.

Finch, J. T. & Holmes, K. C. (1967). In *Methods in Virology* (Maramorosch, K. & Koporowski, H., eds), vol. 3, pp. 351–474, Academic Press, New York.

Franklin, R. E. & Holmes, K. C. (1958). *Acta Crystallogr.* **11**, 213–220.

Guinier, A. (1963). *X-ray Diffraction in Crystals, Imperfect Crystals and Amorphous Bodies*, W. H. Freeman & Co., San Francisco.

Harrison, S. C. (1969). *J. Mol. Biol.* **42**, 457–483.

Harrison, S. C., Caspar, D. L. D., Camerini-Otero, R. D. & Franklin, R. M. (1971). *Nature New Biol.* **229**, 197–201.

Huxley, H. E. & Brown, W. (1967). *J. Mol. Biol.* **30**, 383–434.

Jack, A. & Harrison, S. C. (1975). *J. Mol. Biol.* **99**, 15–26.

Kaiser, A. D., Syvanen, M. & Masuda, T. (1974). *J. Supramol. Struct.* **2**, 318–328.

Karamata, D., Kellenberger, E., Kellenberger, G. & Terzi, M. (1962). *Path. Microbiol.* **25**, 575–585.

King, J. (1968). *J. Mol. Biol.* **32**, 231–262.

King, J. & Casjens, S. (1974). *Nature (London)*, **251**, 112–119.

King, J., Lenk, E. V. & Botstein, D. (1973). *J. Mol. Biol.* **80**, 697–731.

Lenk, E. V., Casjens, S., Weeks, J. & King, J. (1975). *Virology*, **68**, 182–199.

Levine, M. (1972). *Current Topics Microbiol. Immunol.* **58**, 135–156.

Luzzati, V. & Nicolaieff, A. (1959). *J. Mol. Biol.* **1**, 127–133.

Maniatis, T., Venable, J. H., Jr & Lerman, L. S. (1974). *J. Mol. Biol.* **84**, 37–64.

Matthews, B. W. (1974). *J. Mol. Biol.* **82**, 513–526.

Moody, M. F. (1973). *J. Mol. Biol.* **80**, 613–635.

North, A. C. T. & Rich, A. (1961). *Nature (London)*, **191**, 1242–1245.

O'Farrell, P., Gold, L. & Huang, W. (1973). *J. Biol. Chem.* **248**, 5499–5501.

Perutz, M. F. (1946). *Trans. Farad. Soc. B*, **42**, 187–195.

Rhoades, M., MacHattie, L. A. & Thomas, C. A. (1968). *J. Mol. Biol.* **37**, 21–40.

Simon, L. (1972). *Proc. Nat. Acad. Sci., U.S.A.* **69**, 907–911.

Tunis, M. J. B. & Hearst, J. E. (1968). *Biopolymers*, **6**, 1325–1341.

Tye, B., Huberman, J. & Botstein, D. (1974). *J. Mol. Biol.* **85**, 501–532.